REVISION 1

Correction date April 30

Synthesis and structure of carbonated barium and lead fluorapatites: effect of cation size on A-type carbonate substitution

Zachary Wilt,[1] Caitlyn Fuller,[1] Taia Bachman,[1] Victoria Weidner,[1] Jill D. Pasteris,[2] and Claude H. Yoder[1*]

[1]Franklin and Marshall College, Department of Chemistry, Lancaster, PA 17603

[2]Washington University in St. Louis, Department of Earth and Planetary Sciences, St. Louis, MO 63130-4899

[*]To whom correspondence should be addressed. Email: claude.yoder@fandm.edu

Running title: A-type carbonate in barium and lead apatites

Submitted to *American Mineralogist*, October, 2013

ABSTRACT

Substitution of carbonate has long been recognized in both synthetic and natural biologically and geologically precipitated forms of hydroxylapatite. Although the predominant substitution mechanism in all of the calcium members of the apatite group formed below 100 °C is substitution of carbonate for phosphate (B-type), small amounts of A-type substitution of carbonate in the channel sites also occur. The present study focuses on the effect of cation size on the type of substitution of carbonate in members of the apatite group. The barium and lead members offer a larger channel site, which potentially could stabilize A-type substitution. A series of carbonated barium and lead fluorapatites were synthesized in aqueous solution and characterized by powder X-ray diffraction, and infrared and Raman spectroscopy. Carbonate content was determined by combustion analysis.

Unit-cell parameters derived from X-ray diffraction showed that, as carbonate content increased, the **a**-axis length decreased and the **c**-axis increased slightly for carbonated barium fluorapatites (CBaApF), whereas the lengths of both the **a**- and **c**-axes increased for CPbApF. The co-occurrence of two sets of peaks in the ν_3 carbonate region of the infrared spectra of lead and barium carbonated apatites are strongly suggestive of both A- and B-type carbonate substitution. This interpretation is supported by Rietveld analysis of X-ray powder diffraction data, which confirms the presence of significant, but not dominant, A-type substituted carbonate ions. The variation in cell parameters as a function of carbonate substitution mode is discussed, and it is shown that B-type carbonate substitution need not be accompanied by a decrease in the **a**-axis in all apatites. The greater amount of A-type carbonate substitution in barium and lead fluorapatites compared to the their calcium homologs can be attributed to: a) the less negative

enthalpies of hydration of the barium and lead ions relative to that of calcium, and/or b) the greater amount of space available for the relatively large carbonate ions in the channels defined by these large cations. Thus, the substitution modes can be controlled by either thermodynamic or kinetic considerations.

Key words: apatite, Type A-carbonate, Rietveld, infrared, barium apatite, lead apatite

INTRODUCTION

Only five cations form well-characterized end-member apatites. These elements are the alkaline earth metals Ca, Sr, and Ba, the Group 14 metal Pb, and the transition metal Cd (Pan and Fleet 2002; Flora et al. 2004). The barium and lead apatites are particularly interesting because they contain the largest cations (the six-coordinate ionic radii for Ba^{2+} and Pb^{2+} are 1.35 and 1.19 Å, respectively, whereas the radius of Ca^{2+} is 1.00 Å (Shannon 1976)) present in end-member apatites and therefore can provide information on how cation size affects the structure and other characteristics of apatites. Of particular interest are the carbonated forms of these compounds because of the biological importance of the carbonated calcium homolog (CCaApOH), which is the mineral component of bones and teeth, and the possibility that larger cations may influence the substitution mode of carbonate. The barium and lead apatites are also of interest because of their formation in the remediation of heavy metal spills using phosphate remediants (Nriagu 1984; Ruby et al. 1994; Traina and Laperche 1999). We have previously reported on the preparation and characterization of lead hydroxyl- and chlorapatites (pyromorphites) (Sternlieb et al. 2010) as well as barium hydroxyl- and chlorapatites (Yoder et al. 2012).

Carbonate can be incorporated in the apatite structure in two different ways. In A-type substitution, carbonate resides in the channels between the M(2) metal ions, as represented, for example, by the formula $Ca_{10}(PO_4)_6(CO_3)_x(F)_{2-2x}$. In B-type substitution, carbonate replaces a phosphate ion. Both types of substitution require charge compensation due to the difference in charge between the carbonate ion and the ions it replaces. In A-type substitution the charge is generally compensated by the removal of two fluoride ions for each substituting carbonate. There is evidence for two positions of carbonate in the channels—the plane of A1 carbonate ions is parallel to the **c**-axis, while the plane of A2 carbonate ions is nearly perpendicular to the **c**-axis. A2 substitution appears to be correlated with substitution of carbonate for phosphate (Fleet and Liu 2004, Tacker 2008). For B-type substitution a variety of charge-compensation mechanisms have been proposed (Pan and Fleet 2002), but the two most likely for apatites prepared in aqueous solution are a) paired creation of divalent cation and monovalent anion vacancies and b) substitution of sodium ions for channel calcium ions in solutions bearing sodium reagents (Pan and Fleet 2002). The more common mechanism of charge-compensation with vacancy of both a channel metal ion and a monovalent channel anion for B-type substitution is represented, for example, as $Ca_{10-x}(PO_4)_{6-x}(CO_3)_x(F)_{2-x}$. For calcium hydroxyl- and fluorapatites precipitated at temperatures from 20 to 100 °C in aqueous solution, B-type substitution predominates, although some A-type substitution, typically <15% of all carbonate (Elliott 2002), is generally also present. B-type substitution produces a decrease in the **a** unit cell dimension with increasing carbonate incorporation. This change in the **a**-axis length as a function of carbonate content, as observed in calcium fluor- and hydroxylapatites has become an important criterion for recognizing the substitution type—a decrease in **a**-axis length for B-type

substitution and an increase in **a**-axis length for A-type substitution. (LeGeros et al. 1969; Elliott 1994; Pan and Fleet 2002)

Although at least one study has been performed on samples of barium fluorapatite synthesized at high temperature (Meegoda et al. 1999), there appears to be only one report of a synthesis for this apatite in aqueous solution (Flora et al. 2004). Syntheses of lead fluorapatite in aqueous solution (Bhatnagar 1970) and in the solid state (Liu et al. 2008) have been reported.

Our objectives in this study were to prepare barium and lead fluorapatites with varying degrees of carbonation and to determine the substitution mode employed by these compounds to incorporate carbonate. Of particular interest to us was the effect of the nature and size of the cation on the distribution of carbonate in the apatite structure. We have used infrared and Raman spectroscopy as well as Rietveld analysis of XRD patterns to characterize the samples and to determine the location of the carbonate ion in the apatite structure.

EXPERIMENTAL METHODS

All syntheses utilized Milli-Q deionized water through which N_2 had been bubbled for at least 6 hours to remove CO_2. Reagents were ACS reagent grade of purity higher than 98%.

Synthesis of Carbonated BaApF

In order to minimize exposure to atmospheric CO_2, syntheses were performed under a positive pressure of argon, and suction filtration and drying were done in a nitrogen-filled glove bag. Solutions of NH_4F and $(NH_4)_2HPO_4$ were combined before addition of other components.

A solution of the metal nitrate and the solution of NH_4F and $(NH_4)_2HPO_4$ were added simultaneously to a solution of $NaHCO_3$ maintained at 80-90°C. The amount of $NaHCO_3$ was varied to produce apatites with different concentrations of carbonate. Before titration, the pH of the carbonate bath was adjusted to pH 12 using 6 M NaOH solution. During the titration at a rate of 0.05 mL/s, the solution was stirred and the pH was maintained at 12. After ca. 3 hours, the reaction mixture was allowed to sit for 16 h at 85 °C with stirring, under nitrogen. After cooling, the white precipitate was suction filtered in a glove bag using a medium porosity filter crucible, washed thoroughly with three portions of water, allowed to aspirate for an hour, dried with nitrogen in a glove bag for 16 h, and finally heated in a 140°C oven for 1 hour. Percent yields were generally above 80%.

For the preparation of an apatite using a mole ratio of carbonate to phosphate of 0.5 to 1 the following masses of reagents and volumes of water were used for solution preparation: $NaHCO_3$, 0.1345 g, 20 mL; NH_4F, 0.0793 g, 10 mL; $(NH_4)_2HPO_4$, 0.4248 g, 10 mL; $Ba(NO_3)_2$, 1.4018 g, 20 mL.

Synthesis of CPbApF

Portions (25 mL) of solutions of 0.15M $Pb(NO_3)_2$, 0.06M NH_4F, and 0.09M $NH_4H_2PO_4$ were titrated into 100 mL of water at a rate of about 0.7 mL/min. To the solution, 25 mL of different NH_4HCO_3 concentrations were titrated at a rate of 0.7 mL/min to obtain different carbonate/phosphate ratios. The NH_4HCO_3 solution was added at the same time as the other reagents. As the reagents were added, the solution was heated to 80°C, brought to pH 9, and

stirred magnetically. The pH was held at 9 throughout the synthesis with 6M NH_3. After all of the reagents were added, the solution was digested for 2 hours and then was suction filtered. The reaction mixture was filtered using a fine porosity glass filter crucible and was washed with three portions of water. The sample was then dried in vacuo in a vacuum desiccator for over 24 hours. Yields were 80- 95%.

Compositional and structural analyses of samples

Powder X-ray diffractograms were obtained using a PANalytical X'Pert PRO MPD (Multi-Purpose Diffractometer) Theta-Theta System with Cu-Kα radiation. A step size of 0.02° 2-theta was used with a range from 5 to 90° 2-theta. X-ray diffraction was used to confirm the identity of the compound, to detect other phases present in the samples, and to provide data for Rietveld analyses. Data for Rietveld analyses were collected with the sample in a 10 mm silicon cavity mount and scans (ca 5-8 h) sufficient to obtain 60,000 to 100,000 counts.

Unit cell parameters were determined both during Rietveld analyses and by using profile-fitting of the entire XRD pattern. The indexing method was usually McMaille (Le Bail 2004), but in some cases the Treor method (Werner et al. 1985) was employed. The unit cell candidate was chosen based on its high figure of merit, symmetry, and absence of un-indexed peaks. Uncertainties in unit cell parameters were generally ± 0.0007, but repeated measurements on the same sample suggest a higher uncertainty of *ca*. ± 0.001 Å.

Weight percent carbon, lead, phosphorus, and fluoride were all determined by Galbraith Laboratories, Knoxville, TN. Weight percent carbon was determined using a C-, H-, N-

161 elemental analyzer after combustion at 950°C in oxygen. The reported carbon concentrations
162 have a relative experimental error of ± 0.3 wt.%.
163
164 Infrared spectra were obtained using a Ge ATR sample mount on a Bruker Tensor 37 IR
165 spectrometer. Each spectrum represents 256 scans at a resolution of 2 cm^{-1}.
166
167 The confocal Raman system from Kaiser Optical (Ann Arbor, Michigan) that was used in
168 this study has an integrated, fiberoptically coupled microscope-spectrometer-detector. The
169 HoloLab Series Research Raman Spectrometer is configured for 532-nm laser excitation and
170 simultaneously records the spectral range of 100 to 4000 Δcm^{-1}. The detector is an Andor high-
171 resolution, thermoelectrically cooled CCD array that provided a resolution of 2.5 cm^{-1}. Powders
172 were analyzed using an Olympus 80x objective with an N.A. of 0.75. Each Raman spectrum is
173 the average of 32 acquisitions of 4 seconds each. Every sample underwent at least 6 analyses.
174 The laser power was 10 mW at the sample surface, and the diameter of the beam was about 1
175 micrometer at the sample surface. The focus was adjusted for maximum signal:noise ratio.
176
177 The presence of fluoride was ascertained using ^{19}F NMR spectroscopy to determine the
178 relative amount of fluoride in several apatites, previously dissolved in nitric acid. A sample of
179 NaF in the same concentration of acid was used as a standard. Spectra were obtained on an
180 Agilent INOVA 500 MHz spectrometer at 25 °C
181
182 **Rietveld Analysis**

183 The Panalytical program X'pert Highscore Plus (version 2.2e) was used to perform
184 Rietveld analyses on all samples. The profile function was Pseudo Voigt with a polynomial
185 background including 5 coefficient parameters and a flat background parameter. The initial
186 models for $P6_3/m$ calcium fluorapatite (Sudarsanan et al. 1972), barium fluorapatite (Mayer it al.
187 1979), and lead fluorapatite (Belokoneva et al. 1982) were obtained from published single crystal
188 X-ray diffraction data. In all refinements, the zero-shift, scale factor, all 5 background
189 coefficients, unit cell parameters, and profile parameters were refined. It was assumed that both
190 B- and A-type substitution could occur within the same unit cell. The possibility of both types of
191 substitution, either independently or as a mixture of both is well-documented (Beshah et al.
192 1990; Schramm et al. 2000; Tonegawa et al. 2000; Ikoma et al. 2001; Fleet et al. 2004; Astala
193 and Stott 2005; Fleet and Liu 2005; Resende et al. 2006; Nassif et al. 2010). For B-type
194 carbonate the model developed by Wilson et al. (2004) was adopted: the planar carbonate ion
195 was assumed to occupy a face of the tetrahedron that otherwise would have been a phosphate
196 ion, with two of carbonate's oxygen atoms in similar positions to those of the phosphate's
197 oxygen atoms. The occupancies of these two oxygens were not refined. A-type carbonate was
198 assumed to be centered at the position 0, 0, 0.5 with two of the oxygen atoms of the trigonal
199 planar carbonate ion located close to the z-axis, as discussed by Fleet and Liu (Fleet and Liu
200 2005) as the A1 type carbonate. The occupancies of the carbon and its corresponding oxygen
201 sites in A-type substitution were constrained so that the magnitudes of their values changed
202 together.
203
204 To develop a starting model for the refinements, the occupancies were set to values obtained
205 from the formula for B-type substitution as calculated from the analytically-determined

carbonate percentage. These occupancies were then refined, which allowed for a refinement independent of the data obtained from chemical analysis. The occupancies of the carbon and phosphorus could be determined with a lack of divergence, but these occupancies exhibited a great deal of uncertainty. The position of the monovalent anion along the z-axis and its site occupancy were refined in all apatites. The bond lengths in the phosphate tetrahedra and other atomic distances obtained by refinement were very close to those in the starting model. Throughout all refinements, the agreement indices were monitored to be sure that the system was not diverging and that the refinement was moving toward a reasonable representation of the actual structure.

RESULTS AND DISCUSSION

Syntheses

The preparation of both the lead and barium carbonated fluorapatites was accomplished by addition of phosphate and fluoride to a solution of the cation at a pH of 9 and 12, respectively. It is believed that these pH values are optimal. The low solubility of the carbonated lead apatites allows for the formation of those compounds under conditions where the concentration of PO_4^{3-} ion is low. The greater solubility of the barium compared to the lead apatites requires higher pH values to ensure higher concentrations of phosphate. Of course, the much greater solubility of $Ba(OH)_2$ relative to $Pb(OH)_2$ also permits the use of higher pH values in the synthesis of the barium apatites.

X-ray diffraction

The powder X-ray diffraction patterns of carbonated barium fluorapatites show little change in either position or breadth of the peaks with increasing carbonate content. The full width at half maximum (FWHM) for two barium flluorapatites containing 1.3 and 3/0 wt.% carbonate were 0.10 and 0.17, respectively, for the 300 line and 0.20 and 0.20 two theta, respectively, for the 113 line. In contrast, the lead fluorapatites show a relatively small change in the breadth of the peaks, but a definite shift in multiple peak positions to higher two-theta values as the carbonate content increases. For lead fluorapatites containing 1.5 and 3.0 wt% carbonate the FWHM values for the 112 peak were 0.25 and 0.30, respectively, and for the 300 peak 0.32 and 0.37 two theta, respectively. Therefore, unlike their calcium analogs, which show significant peak broadening with increased carbonate content (Nelson and Williamson 1982; Rey et al. 1991), the barium and lead analogs apparently do not undergo major changes in crystallite size and internal strain as carbonate percentages increase. This lack of significant peak broadening was also observed for carbonated barium hydroxyl- and chlorapatites (Yoder et al. 2012).

Unit cell parameters

The unit cell parameters obtained for CBaApF are shown in Figure 1, which demonstrates a decrease in the **a**-axis length of about 0.05Å and a more scattered, but probable increase in **c**-axis length of about 0.01 Å over a range of ca 3 wt. % carbonate. For CPbApF, the unit cell parameters (Fig. 2) show an increase in both axes and hence an increasing cell volume as carbonate content increases, consistent with the observed shifts in all XRD peaks to lower 2 theta values.

A decrease in **a**-axis length was observed previously for CBaApCl, CBaApOH, and CPbApCl, but not in CPbApOH (Yoder et al. 2012; Sternlieb et al. 2010). The decrease in **a**-axis length for CBaApF could be attributed to B-type substitution of carbonate for phosphate, as observed for calcium apatites, but Rietveld analysis and IR spectroscopy (see below) indicate the likelihood of significant A-type substitution (Holcomb and Young 1980; Elliot 2001; Tonegawa et al. 2002; Fleet et al. 2004)

Raman spectra

The Raman spectra of the same samples also show clearly defined peaks for P-O and C-O vibrations. Figure 3 displays the 870 to 1100 Δcm^{-1} region for five CPbApF samples of different carbonate composition. The peaks at 927-933 Δcm^{-1} correspond to the ν_1 symmetric P-O stretching mode and those at 948-967 Δcm^{-1} to the ν_3 asymmetric P-O stretching mode. The intensity of the peaks in the 1039-1050 Δcm^{-1} range correlate with the concentration of carbonate in the samples. All the above peaks are approximately 30 cm^{-1} lower than the corresponding peaks in the calcium analogs, indicating that the cation mass difference controls the relative peak positions. Reference to carbonated hydroxylapatite, CCaApOH (Penel et al. 1998), indicates that the peak at ~1050 Δcm^{-1} can be assigned to B-type carbonate substitution, which is the dominant substitution mechanism recorded in all the Raman spectra. The CPbApF spectra in Figure 3 show not only an increase in intensity of the ~1050 Δcm^{-1} peak with increasing carbonation but also a gradual upshift in peak position, from ~1039 Δcm^{-1} in the uncarbonated apatite. Similar spectral behavior occurs in CCaApOH samples of increasing carbonate concentration, although in that case the carbonate peak downshifts several wavenumbers (Wopenka and Pasteris 2005).

These two peak-shift responses are unexpected for a simple ν_1 C-O symmetric stretch, as each of the carbonate-correlated peaks is often assigned. Instead, the change in peak position in response to additional carbonate incorporation is more suggestive of a band that reflects the interaction between two modes, i.e., a ν_1 C-O and a ν_3 P-O mode (Nelson and Williamson 1982; Penel et al. 1998; Wopenka and Pasteris 2005; Awonusi et al. 2007). In analogy with CCaApOH (Nelson and Williamson 1982; Penel et al. 1998), the weak peak at 1073 Δcm^{-1} is assigned to A-type carbonate, and several other peaks at lower frequency may represent A-type substitution. The Raman spectral response of PbApF to increasing degrees of carbonation is similar to that of CPbApOH (Sterlieb et al. 2010) except for the much greater shift of the ν_1 and ν_3 P-O peak positions in CPbApF. Both CPbApOH and CPbApF show peaks for both A- and B-type carbonate substitution, with B-type strongly dominant.

All of the CPbApF samples also show a broad water peak at about 3400 Δcm^{-1} that dominantly records adsorbed water, but also shows some structural water (Pasteris et al. 2014). A weak sharp peak at 3570 Δcm^{-1} (not shown) in the least carbonated samples corresponds to OH^- ions that presumably occupy the channel. For comparison, the O-H stretch in hydrocerrusite is at 3537 Δcm^{-1}, whereas the O-H stretch in hydroxylapatite is at 3572 $\Delta cm^{-11}$and in PbApOH at 3561 Δcm^{-1} (Sternlieb et al. 2010). The presence of fluoride in the channel site of an OH-bearing apatite phase will displace the O-H stretch peak. Fluoride typically downshifts the peak position due to strong hydrogen bonding in the OH-F interaction, whereas carbonate substitution causes upshift in the O-H stretch of CCaApOH (Pasteris et al. 2012). Thus, the position of the OH peak shown by the least carbonated CPbApF samples may reflect two opposing deflections.

296

297 In the Raman spectra of CBaApF (Fig. 4), the ν_1 P-O stretching mode appears at about the
298 same location as that in CPbApF (935 Δcm^{-1} for CBaApF), but the former's peak position is
299 relatively insensitive to the concentration of carbonate in the sample. However, the width of the
300 ν_1 P-O stretching mode increases as carbonate content increases. This spectral response is similar
301 to that of CBaApOH (Yoder et al., 2012). In CBaApF, the ν_3 mode at 1030 Δcm^{-1} is better
302 resolved than in CPbApF. The intensity of the 1058 Δcm^{-1} peak again indicates the dominance
303 of B-type carbonate substitution compared to the shoulder at ~1075 Δcm^{-1}, which appears to
304 represent A-type substitution.

305

306 The inset in Figure 4 makes clearer the sensitive intensity response of the 1058 Δcm^{-1} peak
307 to carbonate substitution, as well as the slight peak shifts among the ν_3 modes at lower
308 wavenumbers. As with the lead apatites, CBaApF exhibits a broad peak (not shown) centered at
309 about 3400 Δcm^{-1} for the OH stretching of water (mostly adsorbed), but its intensity is not
310 significant except in the most highly carbonated sample. There is no evidence of OH^- ions.

311

312 The Raman spectra of the two sets of samples confirm the purity of the CPbApF and
313 CBaApF powders. Both phases show a significant component of A-type carbonate substitution
314 (not readily quantifiable), but B-type substitution strongly dominates in both. The CPbApF
315 phase shows a greater degree of structural/atomic disorder in response to carbonate substitution
316 than does the CBaApF, as indicated by the greater peak-broadening in the former. The large
317 amount (6 cm^{-1}) of shift in the position of the ν_1 P-O peak in CPbApF (Fig. 3) also indicates

significant change in the phosphate environment due to carbonate substitution, further distinguishing it from CBaApF. In this regard, the Raman data are consistent with the comparative XRD results on the two phases.

Rietveld analysis

Tables 1-3 show the results of Rietveld analyses of the XRD patterns of three series of apatites (CCaApF, CBaApF, and CPbApF) containing low, medium, and high percentages of carbonate. Our Rietveld analyses for three CCaApF apatites were included to provide a control group to demonstrate the general validity of the models used. The atomic coordinates obtained in these analyses are provided in Table 3, and a summary of refinement parameters, cation occupanicies, and bond lengths based on the Rietveld results are given in Table 1 and 2. In Table 1 the column "Total counts/difference counts" provides a ratio of the maximum counts of the experimental XRD pattern to the maximum counts obtained when the pattern developed by the refinement is subtracted from the experimental pattern. This is a measure of the agreement between the experimental and refinement-based X-ray patterns. A more widely used agreement index is R_{wp}, for which values below 6 or 7 % are generally considered to be indicative of satisfactory fits of the data (Wilson et al. 2006; Wilson et al. 2004; Wilson et al. 2005): the lower the R_{wp} value, the better the fit produced by the refinement. The most important columns in these tables are those that give the occupancies of all of the sites in the refined structure. For the ideal end member BaApF ($Ba_{10}(PO_4)_6F_2$), the occupancies of each of the two types of barium sites -- Ba(1) and Ba(2) -- should be exactly 1.000, meaning that all four possible Ba(1) ions and all six Ba(2) ions

are present in the unit cell. The total number of each type of atom can be obtained by multiplying the occupancy by the numerical part of the Wykoff symbol for the atom site (see Table 3).

For the carbonated apatites prepared in this study, it is important to remember that each B-type substitution replaces one phosphate ion with one carbonate ion and (according to the accepted mechanism) results in the loss or vacancy of one calcium ion and one monovalent ion in order to maintain charge neutrality. A-type substitution, on the other hand, results in the displacement of two monovalent channel anions for each substituting carbonate ion. Hence, pure A-type substitution does not change the occupancies of the cation sites, which would remain at 1.000, but decreases the occupancies of the monovalent (X) ions. The type of substitution is also monitored by the occupancies of the two types of carbons belonging to the two structurally distinct types of carbonate ion that could be present in the structure -- C1 (A1-type carbonate in the anion channel) and C2 (B-type carbonate in the phosphate site).

Thus, for the most carbonated calcium control sample CCaApF Table 3 shows occupancies of 0.02(2) for C1 (total of 0.24 A-type carbonate ions), 0.15 for C2 (total of 1.9 B-type carbonate ions), 1.11(7) for Ca1 (total of 4.44 Ca1 cations), 0.96(8) for Ca2 (total of 5.76 Ca2 cations), 0.6(1) for F1 (total of 1.2 fluoride ions), and 0.71(6) for P1 (total of 4.4 phosphate ions). The occupancies for C1 and C2 indicate predominant B-type substitution as does the presence of 4.4 phosphate ions, but the high occupancies of the two types of calcium sites indicate A-type substitution, in which no cations are lost. Table 1 also indicates, however, that the isotropic thermal B_{iso} values for these cations, particularly Ca1, are very high. High B_{iso}

values are generally an indication of high uncertainty in the position and occupancy of an atom. We therefore give less credence to the Ca1 site occupancy and note that substitution of 1.9 B-type carbonate ions (as indicated by the C2 occupancy) should result in loss of the same number of phosphate ions. Hence, the P1 occupancy should be about 6 – 1.9 = 4.1, in acceptable agreement with the value of 4.4 phosphate ions. The large uncertainties associated with each occupancy are also indicative of a great deal of uncertainty in the position of the carbonate in the final refined structure.

Because the most carbonated samples of CBaApF and CPbApF most clearly show A-type substitution in their infrared spectra (see below), we will only analyze the Rietveld occupancies of these two apatites. Thus, CBaApF containing 2.51 wt.% carbonate shows significant occupancy of the channel C1 site (0.07(3)), though this occupancy is only one-quarter that of the B-type C2 site (0.3(2)). There are also large uncertainties associated with both values. The two barium ion site occupancies of 0.9 each indicate a total vacancy of one barium ion, probably produced by B-type substitution. The fluoride occupancy of 0.3 represents 1.4 fluorine site vacancies, which is consistent with both A- and B-type substitution. The phosphorus occupancy of 0.8 corresponds to 1.2 phosphate vacancies, corresponding to dominant B-type substitution.

For CPbApF containing 2.72 wt.% carbonate, the refinement produced one of the largest C1/C2 site occupancy ratios (0.06/0.1), and thus the largest A- to B-type substitution ratios. Even in this case, however, A-type substitution is only about half that of B-type substitution. The “high” P1, Pb1, and Pb2 and low F1 occupancies are consistent with a significant amount of A-type carbonate. We interpret these data as indicative of a greater ratio of A-type substitution

for the barium and lead apatites than that present in CCaApF, but clearly this interpretation is not definitive because of the large uncertainties associated with most of the occupancies.

Infrared spectra

The infrared spectra of the CBaApF and CPbApF samples with varying carbonate concentrations are shown in Figures 5 and 6, where the IR-active carbonate band (ν_3, asymmetric stretch) is about 90 cm^{-1} lower in frequency than the analogous band in CCaApF (Fig. 7). The peaks for CCaApF containing about 13 wt. % carbonate appear at 1421 and 1465 cm^{-1} with a slight shoulder at about 1500 cm^{-1}, consistent with the assignment of peaks at 1420 and 1462 cm^{-1} to B-type carbonate (Rosseeva et al. 2008; Fleet et al. 2004; see summaries in Tacker 2008).

Comparison of the carbonate regions of CBaApF and CPbApF with that of CCaApF reveals that the peaks for the barium and lead apatites appear at lower frequencies. The low frequency peaks in the carbonate band for CPbApF appear at 1330 and 1382 cm^{-1}, with a significant high frequency shoulder from about 1420 to 1460 cm^{-1}. The peaks for CBaApF occur at 1400, 1418, 1435, and 1458 cm^{-1}. We interpret the high frequency peaks in the spectra of both barium (1435 and 1458 cm^{-1}) and lead apatites (from 1420 to 1460 cm^{-1}) as the asymmetric stretch for A-type carbonate. Indeed, the ~1400 cm^{-1} region for the most carbonated CBaApF (Fig. 5) shows two sets of peaks, presumably a doublet for A-type carbonate at higher frequency than the doublet for B-type carbonate. This difference between the asymmetric carbonate stretching frequencies of A- and B-type substitution in calcium apatites has been well

409 documented (Schramm et al. 2000; Tonegawa et al. 2000; Fleet et al. 2004). For example, Shi, et
410 al. (2005) report A-type carbonate asymmetric stretching modes for dental enamel at 1452-1456
411 cm^{-1}, 1495-1501 cm^{-1}, and 1547-1451 cm^{-1} and B-type carbonate modes at 1412-1414 cm^{-1}, and
412 1469-1472 cm^{-1}. Tacker (2008) reports an average of literature B-type carbonate frequencies for
413 synthetic calcium apatites as 1420 ± 6 and 1458 ± 5 cm^{-1}, and for A-type carbonate as 1462 ± 5
414 and 1535 ± 6 cm^{-1}. For geological apatites, Tacker (2008) reports averaged peak maxima of type
415 B1 at 1409 ± 6 and 1450 ± 5 cm^{-1}, type B2 at 1427 ± 1 and 1460 ± 2 cm^{-1}, type A1 at 1539 ± 3
416 and 1475 ± 8 cm^{-1}, and type A2 at 1571 ± 3 and 1499 ± 5 cm^{-1}, and also stresses peak overlap as
417 a source of error in reported peak frequencies.

418 In our spectra of the barium and lead fluorapatites there is no suggestion of additional
419 peaks that could be attributed to a second, conformationally distinct, A-type carbonate as
420 suggested by Fleet (2003, 2004, 2005). The IR spectra of both the barium and lead fluorapatites
421 show very weak broad peaks centered about 3400 cm^{-1}, attributable to water, but no peak at ca.
422 3570 cm^{-1} indicative of hydroxide ions.

423

424

425

426 **RATIONALIZATION OF CELL PARAMETERS AND SUBSTITUTION MODE**

427 Both Rietveld and IR analyses indicate a significant amount of A-type substitution in
428 both CPbApF and CBaApF. For CPbApF, A-type substitution is also indicated by the increase
429 in **a**- and **c**-axis lengths as carbonate content increases. Although it is difficult to provide a more

quantitative assessment, it is clear that the amount of A-type substitution in both of these carbonated barium and lead fluorapatites is greater than that present in CCaApF.

Association of the increase in **a**- and **c**-axis lengths for CPbApF with A-type carbonate substitution is consistent with the long-held belief that an increase in **a**-axis (but a slight decrease in **c**-axis) length in calcium apatites is due to the replacement of the monovalent anion (usually OH^- or F^-) with the larger carbonate ion (Holcomb and Young 1980; Elliot 2002; Fleet et al. 2004; Tonegawa 2010). However, the clear dominance of B-type substitution in CPbApF seems to make this explanation less plausible. Assuming that the basic hexagonal structure of the apatite is maintained, the increase in both axial lengths must result from additional volume in the crystal structure necessitated by the increasing incorporation of the carbonate ion. Examination of atomic distances in the Rietveld-refined structures of CPbApF with 0.2 wt.% and 2.7 wt.% carbonate shows that the primary differences lie in the distances between the triangularly disposed Pb(2) ions lying within planes perpendicular to the **c**-axis: the distance between these channel-defining ions is about 6% greater in the more carbonated apatite. By comparison, the closest distances between Pb(1) atoms are only 1.4% greater in the more carbonated apatite. This analysis indicates widening of the channels, which correlates with the increase in the length of both axes. Such widening may result from replacement of fluoride by carbonate (A-type substitution). However, it also may be the case that greater B-type substitution produces a widening of the channels in the lead fluorapatites; that is, even when the carbonate ion does not occupy the channels, but substitutes for phosphate, the channels may widen significantly. Increased substitution of carbonate for phosphate with its concomitant development of fluoride vacancies within the channel may produce greater repulsions (due to loss of attraction to

453 fluoride) between the channel-bounding lead ions. This channel expansion may be pronounced
454 in CPbApF because of possible channel-delimiting, dative interactions between fluoride ions and
455 the Lewis acidic lead cations, which would disappear as B-type substitution occurs. The same
456 explanation may account for the observed (Sternlieb et al. 2010) increase in the **a**-axis length
457 with increasing carbonate incorporation in CPbApOH.
458
459 In contrast to the effect of carbonate on the **a**-axis length in CPbApF, the **a**-axis length of
460 CBaApF decreases uniformly with an increase in carbonate substitution. For this Ba apatite both
461 Rietveld analysis and infrared spectroscopy indicate that A-type carbonate substitution is a
462 substantial portion of the total substitution, but less than that in the lead analog. The decrease in
463 the **a**-axis length in CBaApF (in which the proportion of A-type substitution is less than that in
464 the lead analog) with increasing carbonate incorporation, can be explained by the smaller amount
465 of A-type carbonate, by the absence of dative interactions of fluoride ions with the non Lewis
466 acidic barium ions, or by both effects.
467
468 Our IR and Rietveld analyses suggest that A-type carbonate substitution is more
469 prevalent in barium and lead fluorapatites than in the smaller cation analog CCaApF, an
470 observation that can be rationalized by the larger channels present in the barium and lead
471 compounds. The differences in volume available in the channel can be estimated in two
472 dimensions by considering one plane of M(2) ions. The areas of the arcs produced by the M(2)
473 ions, obtained using standard formulas along with 6-coordinate ionic radii (Shannon 1976) and
474 the 60° angle within the arc, are subtracted from the area of the triangle. The resulting "free
475 space" in two dimensions provides an estimate of the space within the M(2) triangles in the

absence of a monovalent anion. Using distances obtained from the structures of CaApF (Wyckoff 1965) and BaApF (Mathew et al. 1979) we estimate their free areas to be 4.6 $Å^2$ and 5.5 $Å^2$, respectively, an increase in area of 20% in moving from Ca^{+2} to Ba^{+2}. Thus, we assume that A-type substitution is either more energetically favorable or kinetically more viable for apatites that contain larger cations.

Modeling studies of the relative stabilities of the A- and B-type carbonate sites in CCaApOH at 37 °C indicate that A-type (and mixed AB-type) carbonate substitution is energetically more favorable than B-type (Peroos et al. 2006). Assuming that the presumably greater electrostatic interactions in the channel favor A-type substitution even in apatites with larger cations, we speculate that in the compounds prepared here, which contain larger cations, A-type substitution is thermodynamically favored. Why, then, do not all apatites, regardless of cation size, contain carbonate only in the channel (though one could imagine compounds with apatitic structures that could contain either extremely large cations or cations of lower charge where the channel site would not be energetically favored)? The answer may lie in the rate of the carbonate-incorporating reaction; that is, the rate at which carbonate substitutes for phosphate may be greater than the rate at which it substitutes for monovalent channel ions during the formation of the carbonated apatite. If these assumptions are correct, they also seem to suggest that during the formation of the carbonated apatite, the channel structure has already formed before the carbonate enters the mechanistic sequence.

It is also possible that B- type carbonate substitution is favored for most apatites formed in aqueous solution for thermodynamic reasons. Thermochemical analysis of substitution

499 requires an assumption about the charge balance mechanism involved in those substitutions. We
500 find no evidence from Raman, IR, or XRD for the incorporation of sodium in our products. We
501 have also done sodium analyses for calcium apatites prepared with the same procedure used for
502 the syntheses of the barium apatites and have found only ca. 1% sodium in those products.
503 Moreover, the changes in occupancies observed in our Rietveld analysis are consistent with
504 dominant B-type substitution involving creation of calcium and fluoride vacancies. The
505 equations for the most common substitution mechanisms for A-type and B-type carbonate are
506 shown below for the substitution of one mole of carbonate per mole of apatite.

507 A-type: $M_{10}(PO_4)_6F_2(s) + CO_3^{2-}(aq) \rightarrow M_{10}(PO_4)_6(CO_3)(s) + 2\ F^-(aq)$

508 B-type: $M_{10}(PO_4)_6F_2(s) + CO_3^{2-}(aq) \rightarrow M_9(PO_4)_5(CO_3)F(s) + M^{2+}(aq) + PO_4^{3-}(aq) + F^-$
509 (aq)

510

511 Subtraction of the second equation from the first produces:

512 $$M_9(PO_4)_5(CO_3)F(s) + M^{2+}(aq) + PO_4^{3-}(aq) \rightarrow M_{10}(PO_4)_6(CO_3)(s) + F^-(aq)$$

513 B-type A-type

514 which represents the relative "stability" of B-type substitution of one carbonate for phosphate
515 compared to A-type substitution of one carbonate for two fluorides in solution (assuming the
516 charge compensation mechanism shown). The Gibbs energy change for this reaction could be
517 estimated in several ways, one of which is to calculate the lattice enthalpy of both
518 $M_9(PO_4)_5(CO_3)F(s)$ and $M_{10}(PO_4)_6(CO_3)(s)$ and then determine the enthalpy of hydration of the
519 resultant gaseous ions (which form the solvated $M^{2+}(aq)$, $PO_4^{3-}(aq)$, and $F^-(aq)$ ions in the
520 equation above). The resultant $\Delta H°$ could then be converted to $\Delta G°$ using standard techniques
521 for estimating absolute entropies. The lattice enthalpy for A- type apatite can with some

certainty be assumed to be greater (meaning that the potential energy of the A-type apatite is lower and therefore it is more stable) than that of B-type apatite. This assertion rests on the greater number of more highly charged ions in the A-type lattice and the results of molecular dynamics calculations (Peroos et al. 2006). If the enthalpies of hydration of the M^{2+}, PO_4^{3-} and F^- ions are ignored, the $\Delta H°$ (and $\Delta G°$) for the equation above could be assumed to be negative and the formation of A-type apatite in solution could be assumed to be favorable with respect to B-type apatite at least under conditions where the concentrations of the ions in solution are similar.

Our experimental work indicates that for barium and lead fluorapatites B-type substitution is favorable, but less so than for the calcium analog. This difference could be explained by the differences in enthalpies of hydration of the cations (the anions need not be considered because they will be the same no matter what cation is being considered), which in kJ/mol are Ca^{2+} -1577, Ba^{2+} -1305, Pb^{2+} -1481 (Smith 1977). The Gibbs energies of hydration also vary inversely with the ionic radii of the ions (Latimer et al. 1939). The enthalpies (and Gibbs energies) of hydration therefore make $\Delta G°$ for the equation above less favorable for those apatites that contain cations with the most negative enthalpies of hydration. Thus, the greater amount of A-type carbonated apatite for barium and lead fluorapatite compared to calcium fluorapatite can be attributed to the less negative enthalpy (and Gibbs energy) of hydration of the larger Ba^{2+} and Pb^{2+} ions.

The greater percentage of carbonate that resides in the channel sites of the barium and lead fluorapatites, relative to that of carbonated calcium fluorapatite, can therefore be attributed

to an increased rate of incorporation into the more spacious barium and lead cation channels and/or to the thermodynamically-determinant effect of the solvation of the cations. We are continuing to study the consequences of these and similar observations.

IMPLICATIONS

Our work provides structural observations and principles that can be used to understand the incorporation of carbonate in compounds in the apatite family that vary in the size and chemical nature of the cations present. These principles, in turn, are of value in the interpretation of unit cell parameters, particularly their variation with carbonate content, differences in occupancies of different substitution sites, and the nature/importance of the channel structure of apatites. We have shown that apatites with cations larger than calcium may incorporate carbonate more readily in the A- (channel) site and that an increase in the relative amount of A-type substitution is not necessarily revealed experimentally by an increase in the length of the a-axis. We have also provided a thermochemical analysis that can be used for any apatite to understand the relative energetics of A- vs B-type carbonate substitution. These principles may be of value in understanding the composition and compositional variation within bone and tooth material and in the design of apatites that, by virtue of different substitution patterns, may have properties that are of value in, for example, the remediation of heavy metal contamination or the encapsulation of nuclear waste.

ACKNOWLEDGMENTS

The authors acknowledge the Lucille and William Hackman Research Endowment at Franklin and Marshall College and the Center for Materials Innovation at Washington University for

partial funding of this study. This material is based upon work supported by the National Science Foundation under Grant No. 0923224. We are also indebted to Linh Tran and Molly Carney for technical assistance and to the reviewers for their insightful comments.

References Cited

Astala, R., and Stott, M. J. (2005) First principles investigation of mineral component of bone: CO_3 substitutions in hydroxyapatite. Chemistry of Materials, 17, 4125-4133.

Awonusi, A., Morris, M.D., and Tecklenburg, M.M.J. (2007) Carbonate assignment and calibration in the Raman spectrum of apatite. Calcified Tissue International, 81, 46-52.

Bhatnagar, V. M. (1970) Preparation, lattice parameters and X-ray powder patterns of lead fluorapatite and lead chlorapatite, Inorganic and Nuclear Chemistry Letters, 6, 913-917

Belokoneva, E.L., Troneva, E.A., Dem'yanets, L.N., Duderov, N.G., and Belov. N.V. (1982) The crystal structure of synthetic fluoropyromorphite $Pb_5(PO_4)_3F$. Kristallografiya, 27, 793-94.

Beshah K., Rey C., Glimcher M.J., Schimizu M., and Griffin R.G. (1990) Solid state carbon-13 and proton NMR studies of carbonate containing calcium phosphates and enamel. Journal of Solid State Chemistry, 84, 71-81.

Elliot, J. C. (2002) Calcium phosphate biominerals. In Kohn, M. J., Rakovan, J., and Hughes, J.M. Eds, Phoshates—Geochemical, geobiological, and materials importance, 48, p. 427-453. Reviews in Mineralogy and Geochemistry, Mineralogical Society of America, Chantilly, Virginia..

Fleet, M.E., and Liu, X. (2003) Carbonate apatite type A synthesized at high pressure: new space group (P3) and orientation of channel carbonate ion. Journal of Solid State Chemistry, 174, 412–417.

Fleet, M.E., and Liu, X. (2004) Location of type B carbonate ion in type A-B carbonate apatite synthesized at high pressure. Journal of Solid State Chemistry, 177, 3174–3182.

Fleet, M.E., Liu, X., and King, P.L. (2004) Accommodation of the carbonate ion in apatite: an FTIR and X-ray structure study of crystals synthesized a 2-4 GPa. American Mineralogist, 89, 1422-1432.

Fleet, M.E., and Liu. X. (2005) Local structure of channel ions in carbonate apatite. Biomaterials., 26, 7548-554.

Flora, N.J., Hamilton, K.W., Schaeffer, R.W., and Yoder, C.H. (2004) A Comparative Study of the Synthesis of Calcium, Strontium, Barium, Cadmium, and Lead Apatites in Aqueous Solution. Synthesis and Reactivity of Metal-Organic Compounds, 34, 503-521.

Holcomb, D.W., and Young, R.A., (1980) Thermal decomposition of human tooth enamel. Calcified Tissue International, 31, 189-201.

Ikoma, T., Kubo, Y., Yamazaki, A., Akao, M., and Tanaka, J. (2000) Key Engineering Materials. 192-1, 191-94.

Latimer, W. M., Pitzer, K. S., Stansky, C. M. (1939) The free energy of hydration of gaseous ions, and the absolute potential of the normal calomel electrode, Journal of Chemical Physics, 7, 108-111.

Le Bail, A. (2004) Monte Carlo indexing with McMaille, Powder Diffraction, 19, 249-254.

LeGeros, R.Z., Trautz, O.R., Lkein, E., and LeGeros, J.P. (1969) Two types of carbonate substitution in the apatite structure. Experimentia, 25, 5-7.

Liu, X., Shieh, S.R., Fleet, M.E., and Akhmetov, A. (2008) High-pressure study on lead fluorapatite. American Mineralogist, 93, 1581-1584.

Mathew, M., Mayer, I., Dickens, B., and Schroeder, L.W. (1979) Substitution in barium-fluoride apatite: the crystal structures of $Ba_{10}(PO_4)_6F_2$, $Ba_6La_2Na_2(PO_4)_6F_2$ and $Ba_4Nd_3Na_3(PO_4)_6F_2$. Journal of Solid State Chemistry, 28, 79-95.

Meegoda, C., Bonner, C.E., Loutts, G., Stefanos, S., and Miller, III, G.E. (1999) Raman spectroscopic study of barium fluorapatite. Journal of Luminescence, 81, 101-109.

Nassif, N., Martineau, F., Syzgantseva, O., Gobeaux, F., Willinger, M., Coradin, T., Cassaignon, S., Azaïs, T., and Giraud-Guille, M. M. (2010) Chemistry of Materials. 22, 3653-3663.

Nelson, D. G. A., Williamson, B. E., (1982) Low-temperature laser Raman spectroscopy of synthetic carbonated apatites and dental enamel, Australian Journal of Chemistry, 35, 715-727/

Nriagu, J. O. (1984) Phosphate Minerals, Nriagu, J.O., and Moore, P.B., Eds. 318-329, Springer-Verlag, New York.

Pan, Y., and Fleet, M.E. (2002) Composition of the apatite-group minerals: substitution mechanisms and controlling factors. In Kohn, M.J., Rakovan, J., and Hughes, J.M., Eds. Phosphates-Geochemical, geobiological, and materials importance, 48, p. 13-49. Reviews in mineralogy and geochemistry, Mineralogical Society of America, Chantilly, Virginia.

Pasteris, J.D., Yoder, C. H., and Wopenka, B. (2014) Molecular water in nominally unhydrated carbonated hydroxylapatite: the key to a better understanding of bone mineral. American Mineralogist, 99, 16-27.

Pasteris, J.D., Yoder, C.H., Sternlieb, M.P., and Liu, S. 20120. Effect of carbonate incorporation on the hydroxyl content of hydroxylapatite. Mineralogical Magazine, 76, 2741-2759.

Penel, G., Leroy, G., Rey, C., and Bres, E. (1998) MicroRaman spectral study of the PO_4 and CO_3 vibrational modes in synthetic and biological apatites. Calcified Tissue International, 63, 475-481.

Peroos, S., Du, Z., and de Leeuw, N. H. (2006) A computer modeling study of the uptake, structure and distribution of carbonate defects in hydroxyl-apatite. Biomaterials, 27, 2150-2161.

Resende, N.S., Nele, M., and Salim, V.M.M. (2006) Effects of anion substitution on the acid properties of hydroxyapatite. Thermochimica Acta, 451, 16-21.

Rey, C., Renugopalakrishnan, V., Collins, B., Glimcher, M.J., (1991) Fourier transferom infrared spectroscopic study of the carbonate ions in bone mineral during aging, Calcified Tissue International, 49, 251-258.

Rosseeva, E.V., Buder, J., Simon, P., Schwarz, U., Frank-Kamenetskaya, O. V., and Kniep, R. (2008) Synthesis, characterization, and morphogenesis of carbonated fluorapatite-gelatine nanocomposites: a complex biomimetic approach toward the mineralization of hard tissues, Chemistry of Materials, 20, 6003-6013.

Ruby, M.V., Davis, A., and Nicholson, A.D. (1994) In situ formation of lead phosphates in soils as a method to immobilize lead. Environmental Science and Technology, 28, 646-654.

Shannon, R.D. (1976) Revised effective ionic-radii and systematic studies of interatomic distances in halides and chalcogenides. Acta Crystallographica Section A, 32, 751-767.

Schramm, D.U., Terra, J., Rossi, A.M., and Ellis, D. E. (2001) Configuration of CO_2(-) radicals in gamma-irradiated A-type carbonated apatites: theory and experimental EPR and ENDOR studies. Physical Review B, 63, 1-14.

Shi, J., Klocke, A., Zhang, M., and Bismayer, U. (2005) Thermally-induced structural modification of dental enamel apatite: decomposition and formation of carbonate groups. European Journal of Mineralogy, 17, 769-775.

Smith, D. W. (1977) Ionic hydration enthalpies, Journal of Chemical Education, 54, 540-541.

Sternlieb, M.P., Pasteris, J.D., Williams, B.R, Krol, K.A., and Yoder, C.H. (2010) The structure and solubility of carbonated hydroxyl- and chloro lead apatites. Polyhedron, 29, 2364-2372.

Sudarsanan, K., Mackie, P.E., and Young, R.A. (1972) Comparison of synthetic and mineral fluorapatite, $Ca_5(PO_4)_3F$, in crystallographic detail. Materials Research Bulletin, 7, 1331-338.

Tacker R.C. (2008) Carbonate in igneous and metamorphic fluorapatite: two type A and two type B substitutions. American Mineralogist, 93, 168-176.

Tonegawa, T., Ikoma, T., Yoshioka, T., Hanagata, N., and Tanaka, J. (2010) Crystal structure refinement of A-type carbonate apatite by X-ray powder diffraction. Journal of Material Science, 45, 2419-2426.

Traina, S.J., and Laperche, V. (1999) Contaminant bioavailability in soils, sediments, and aquatic environments. Proceedings of the National Academy of Sciences of the United States of America, 96, 3365-3371.

Werner, P.-E., Eriksson, L. and Westdahl, M. J., Journal of Applied Crystallography 18, 367-370.

Wilson R.M., Elliott J.C., Dowker S.E.P., and Smith R.I. (2004) Rietveld structure refinement of precipitated carbonate apatite using neutron diffraction data. Biomaterials, 25, 2205-13.

722 Wilson, R.M., Elliott, J.C., Dowker, S.E.P., and Rodriguez-Lorenzo, L.M. (2005) Rietveld
723 refinements and spectroscopic studies of the structure of Ca-Deficient apatite. Biomaterials.
724 2005, 26, 1317-327.
725
726 Wilson, R.M., Dowker, S.E.P., and Elliott, J.C. (2006) Rietveld refinements and spectroscopic
727 structural studies of a Na-free carbonate apatite made by hydrolysis of monetite.
728 Biomaterials., 27, 4682-692.
729
730 Wopenka, B., and Pasteris, J.D. (2005) A mineralogical perspective on the apatite in bone.
731 Materials Science and Engineering C, 25, 131-143.
732
733 Wyckoff, R.W.G. (1965) Crystal Structures, 2nd Edition, Vol. 3, p. 228, Interscience, New York.
734
735 Yoder, C. H., Pasteris, J.D., Krol, K.A., Weidner, V. L, and Schaeffer, R. W. (2012) Synthesis,
736 structure, and solubility of carbonated barium chlor- and hydroxylapatites. Polyhedron,
737 44, 143-149.
738
739 Yoder, C.H., and Rowand, J.P. (2006) Application of the simple salt lattice energy
740 approximation to the solubility of minerals. American Mineralogist, 91, 747-752.
741
742
743 **Figure Captions**
744

745

746 **Fig. 1**. Variation of unit cell parameters as a function of weight percent carbonate in CBaApF.

747 **Fig. 2**. Variation of unit cell parameters as a function of weight percent carbonate in CPbApF.

748 **Fig. 3**. Raman spectra for five CPbApF samples of varying carbonate composition.

749 **Fig. 4**. The 900 – 1200 Δcm^{-1} region of the Raman spectra of three CBaApF samples. In the
750 inset, the peaks are normalized to the intensity of the ν_3 mode at 1031 Δcm^{-1}, making more clear
751 the increase in intensity of the 1058 Δcm^{-1} peak representing B-type substitution.

752 **Fig. 5**. IR spectrum of CBaApF showing carbonate and phosphate bands in the region between
753 1500 and 900 cm^{-1}. The inset shows the carbonate region.

754 **Fig. 6**. The infrared spectra of CPbApF samples from 700 to 1600 cm^{-1}. The inset shows the
755 carbonate region.

756 **Fig. 7**. The IR spectra of CCaApF samples from 1800 – 750 cm^{-1}.

757

758

759

760 **Table 1**. Rietveld refinement parameters and site occupancies for cations and
761 monovalent anions.

Compound	Wt. Percent CO_3	Ion CO_3 Per Unit Cell	Total Counts: Difference Ratio	R_{wp} (%)	M_1 Occupancy	M_1 B-iso	M_2 Occupancy	M_2 B-iso	X Ions/ Unit Cell
CCaApF	1.45	0.24	5	7.53	1.13(7)	2.5(1)	0.88(6)	0.0(1)	1.6(2)
CCaApF	4.23	0.67	6	6.23	1.13(7)	2.5(2)	0.91(8)	0.0(1)	1.8(2)
CCaApF	13.55	1.88	12.5	4.58	1.11(7)	3.1(1)	0.96(8)	0.9(1)	1.2(2)
CBaApF	0.70	0.23	25	5.04	0.94(9)	0.28(5)	0.92(9)	0.14(4)	1.2(4)
CBaApF	1.31	0.42	13	6.17	1.0(1)	0.68(5)	1.0(1)	0.63(4)	1.2(4)
CBaApF	2.51	0.77	16	6.15	0.9(1)	0.38(5)	0.9(1)	0.57(5)	0.6(4)

CPbApF	0.22	0.10	23	4.51	1.0(2)	0.41(5)	1.0(2)	0.94(4)	1.6(8)
CPbApF	1.59	0.67	21	7.20	1.0(2)	0.97(9)	0.9(2)	1.22(8)	1.0(8)
CPbApF	2.72	1.09	70	4.04	1.0(1)	0.69(4)	0.9(1)	1.35(4)	1.0(4)

762

763 **Table 2**. Selected bond lengths obtained in the Rietveld refinements.

Compound	Wt. Percent CO_3	P_1–O_1 (Å)	P_1–O_2 (Å)	P_1–O_3 (Å)	M_1–O_1 (Å)	M_1–O_2 (Å)	M_1–O_3 (Å)	M_2–X (Å)	M_2–O_2 (Å)	M_2–O_3 (Å)
CCaApF	1.45	1.5385(2)	1.5454(2)	1.5364(2)	2.403(3)	2.454(3)	2.809(1)	2.332(3)	2.366(3)	2.338(1)
CCaApF	4.23	1.5321(2)	1.5390(2)	1.5347(2)	2.396(4)	2.453(4)	2.798(1)	2.293(3)	2.384(3)	2.344(1)
CCaApF	13.55	1.5233(2)	1.5302(2)	1.5331(2)	2.372(4)	2.467(4)	2.787(1)	2.293(3)	2.363(3)	2.340(1)
CBaApF	0.70	1.5382(2)	1.5330(2)	1.5329(2)	2.725(2)	2.710(2)	>3	2.525(1)	2.663(1)	2.739(1)
CBaApF	1.31	1.5370(2)	1.5318(2)	1.5332(2)	2.726(3)	2.710(3)	>3	2.524(1)	2.659(1)	2.741(1)
CBaApF	2.51	1.5336(2)	1.5284(2)	1.5327(2)	2.726(3)	2.706(3)	>3	2.494(1)	2.675(1)	2.747(1)
CPbApF	0.22	1.5564(2)	1.5435(2)	1.5869(2)	2.510(1)	2.728(1)	2.911(1)	2.939(1)	2.383(1)	2.562(1)
CPbApF	1.59	1.5641(2)	1.5511(2)	1.6028(2)	2.52(1)	2.76(1)	2.929(4)	>3	2.322(4)	2.595(2)
CPbApF	2.72	1.5700(2)	1.5570(2)	1.6094(2)	2.542(6)	2.764(5)	2.937(1)	>3	2.309(2)	2.600(1)

764

765

766 **Table 3.** Site occupancies and atomic coordinates for atoms in synthesized CMApF.
767

Compound	Synthesis ID	Percent C Wt. % CO_3^{2-}	Ions CO_3 carbonate ions per unit cell	Atom site	Wyckoff Wyckoff symbol	Site occup. occup.	x Coordinates x	C Coordinates y	z Coordinates z
CCaApF	DSCaApF13	1.45	0.24						
				C1	12i	0.01(2)	0.014000	0.010000	0.019000
				C2	12i	0.0(1)	0.419700	0.013700	0.187000
				Ca1	4f	1.13(7)	0.333333	0.666667	0.0006(7)
				Ca2	6h	0.88(6)	0.2429(4)	0.2532(4)	0.250000
				F1	2a	0.8(1)	0.000000	0.000000	0.250000
				O1	6h	1.000000	0.158100	0.484300	0.250000
				O2	6h	1.000000	0.588000	0.121200	0.250000
				O3	12i	0.8(1)	0.341600	0.084800	0.070400
				O5	12i	0.01(2)	0.105000	0.166500	0.002000
				O6	12i	0.01(2)	0.021000	0.051000	0.187000
				O7	12i	0.01(2)	0.073000	0.001000	0.128200
				P1	6h	0.916064	0.398100	0.029300	0.250000
CCaApF	DSCaApF1	4.23	0.67						
				C1	12i	0.00(2)	0.014000	0.010000	0.019000
				C2	12i	0.0(1)	0.419700	0.013700	0.187000
				Ca1	4f	1.13(7)	0.333333	0.666667	0.0013(8)
				Ca2	6h	0.91(8)	0.2395(4)	0.2502(5)	0.250000
				F1	2a	0.9(1)	0.000000	0.000000	0.250000
				O1	6h	1.000000	0.158100	0.484300	0.250000
				O2	6h	1.000000	0.588000	0.121200	0.250000
				O3	12i	0.79(8)	0.341600	0.084800	0.070400
				O5	12i	0.00(2)	0.105000	0.166500	0.002000
				O6	12i	0.00(2)	0.021000	0.051000	0.187000
				O7	12i	0.00(2)	0.073000	0.001000	0.128200
				P1	6h	0.8(1)	0.398100	0.029300	0.250000
CCaApF	DSCaApF9	13.55	1.88						
				C1	12i	0.02(2)	0.014000	0.010000	0.019000
				C2	12i	0.148461	0.419700	0.013700	0.187000
				Ca1	4f	1.11(7)	0.333333	0.666667	0.0051(8)
				Ca2	6h	0.96(8)	0.2403(4)	0.2523(5)	0.250000
				F1	2a	0.6(1)	0.000000	0.000000	0.250000
				O1	6h	1.000000	0.158100	0.484300	0.250000
				O2	6h	1.000000	0.588000	0.121200	0.250000
				O3	12i	0.7(1)	0.341600	0.084800	0.070400
				O5	12i	0.02(2)	0.105000	0.166500	0.002000
				O6	12i	0.02(2)	0.021000	0.051000	0.187000
				O7	12i	0.02(2)	0.073000	0.001000	0.128200
				P1	6h	0.71(6)	0.398100	0.029300	0.250000
CBaApF	CT5	0.70	0.23						
				Ba1	4f	0.94(9)	0.333333	0.666667	0.0006(4)
				Ba2	6h	0.92(9)	0.2571(1)	0.2391(1)	0.250000
				C1	12i	0.04(2)	0.018000	0.065000	0.008000
				C2	12i	0.1(2)	0.017800	0.419600	0.198000
				F1	2a	0.6(2)	0.000000	0.000000	0.250000
				O1	6h	1.000000	0.482000	0.140400	0.250000
				O2	6h	1.000000	0.117400	0.576000	0.250000
				O3	12i	1.0(1)	0.079100	0.347300	0.088800
				O5	12i	0.04(2)	0.084000	0.208900	0.028000
				O6	12i	0.04(2)	0.007000	0.023000	0.143000
				O7	12i	0.04(2)	0.022000	0.008000	0.139000
				P1	6h	1.0(2)	0.031900	0.401700	0.250000

CBaApF	CT2	1.31	0.42						
				Ba1	4f	1.0(1)	0.333333	0.666667	0.0007(5)
				Ba2	6h	1.0(1)	0.2571(1)	0.2394(1)	0.250000
				C1	12i	0.04(2)	0.018000	0.065000	0.008000
				C2	12i	0.2(2)	0.017800	0.419600	0.198000
				F1	2a	0.6(2)	0.000000	0.000000	0.250000
				O1	6h	1.000000	0.482000	0.140400	0.250000
				O2	6h	1.000000	0.117400	0.576000	0.250000
				O3	12i	1.0(1)	0.079100	0.347300	0.088800
				O5	12i	0.04(2)	0.084000	0.208900	0.028000
				O6	12i	0.04(2)	0.007000	0.023000	0.143000
				O7	12i	0.04(2)	0.022000	0.008000	0.139000
				P1	6h	0.9(2)	0.031900	0.401700	0.250000
CBaApF	CT7	2.51	0.77						
				Ba1	4f	0.9(1)	0.333333	0.666667	0.0011(5)
				Ba2	6h	0.9(1)	0.2548(2)	0.2370(2)	0.250000
				C1	12i	0.07(3)	0.018000	0.065000	0.008000
				C2	12i	0.3(2)	0.017800	0.419600	0.198000
				F1	2a	0.3(2)	0.000000	0.000000	0.250000
				O1	6h	1.000000	0.482000	0.140400	0.250000
				O2	6h	1.000000	0.117400	0.576000	0.250000
				O3	12i	1.0(1)	0.079100	0.347300	0.088800
				O5	12i	0.07(3)	0.084000	0.208900	0.028000
				O6	12i	0.07(3)	0.007000	0.023000	0.143000
				O7	12i	0.07(3)	0.022000	0.008000	0.139000
				P1	6h	0.8(2)	0.031900	0.401700	0.250000
CPbApF	ZW11	0.22	0.10						
				C1	12i	0.06(3)	0.018000	0.065000	0.008000
				C2	12i	0.3(3)	0.412000	0.004000	0.187000
				F1	2a	0.000000	0.000000	0.000000	0.250000
				O1	6h	1.000000	0.164000	0.487000	0.250000
				O2	6h	1.000000	0.582000	0.096000	0.250000
				O3	12i	0.8(2)	0.347000	0.080000	0.078000
				O5	12i	0.06(3)	0.068200	0.212200	0.028000
				O6	12i	0.06(3)	0.007000	0.005000	0.152000
				O7	12i	0.06(3)	0.024000	0.010000	0.148000
				P1	6h	0.9(2)	0.400400	0.019100	0.250000
				Pb1	4f	0.8(1)	0.333333	0.666667	-0.001(2)
				Pb2	6h	0.8(1)	0.2376(3)	0.2348(3)	0.250000
CPbApF	ZW12	1.59	0.67						
				C1	12i	0.06(4)	0.018000	0.065000	0.008000
				C2	12i	0.3(4)	0.412000	0.004000	0.187000
				F1	2a	0.000000	0.000000	0.000000	0.250000
				O1	6h	1.000000	0.164000	0.487000	0.250000
				O2	6h	1.000000	0.582000	0.096000	0.250000
				O3	12i	0.7(2)	0.347000	0.080000	0.078000
				O5	12i	0.06(4)	0.068200	0.212200	0.028000
				O6	12i	0.06(4)	0.007000	0.005000	0.152000
				O7	12i	0.06(4)	0.024000	0.010000	0.148000
				P1	6h	0.8(3)	0.400400	0.019100	0.250000
				Pb1	4f	0.8(2)	0.333333	0.666667	-0.001(2)
				Pb2	6h	0.8(2)	0.2491(6)	0.2485(5)	0.250000
CPbApF	ZW3	2.72	1.09						
				C1	12i	0.06(3)	0.018000	0.065000	0.008000
				C2	12i	0.1(3)	0.412000	0.004000	0.187000
				F1	2a	0.000000	0.000000	0.000000	0.250000
				O1	6h	1.000000	0.164000	0.487000	0.250000
				O2	6h	1.000000	0.582000	0.096000	0.250000

O3	12i	0.7(1)	0.347000	0.080000	0.078000
O5	12i	0.06(3)	0.068200	0.212200	0.028000
O6	12i	0.06(3)	0.007000	0.005000	0.152000
O7	12i	0.06(3)	0.024000	0.010000	0.148000
P1	6h	1.0(2)	0.400400	0.019100	0.250000
Pb1	4f	1.0(1)	0.333333	0.666667	-0.003(1)
Pb2	6h	0.9(1)	0.2472(4)	0.2474(3)	0.250000

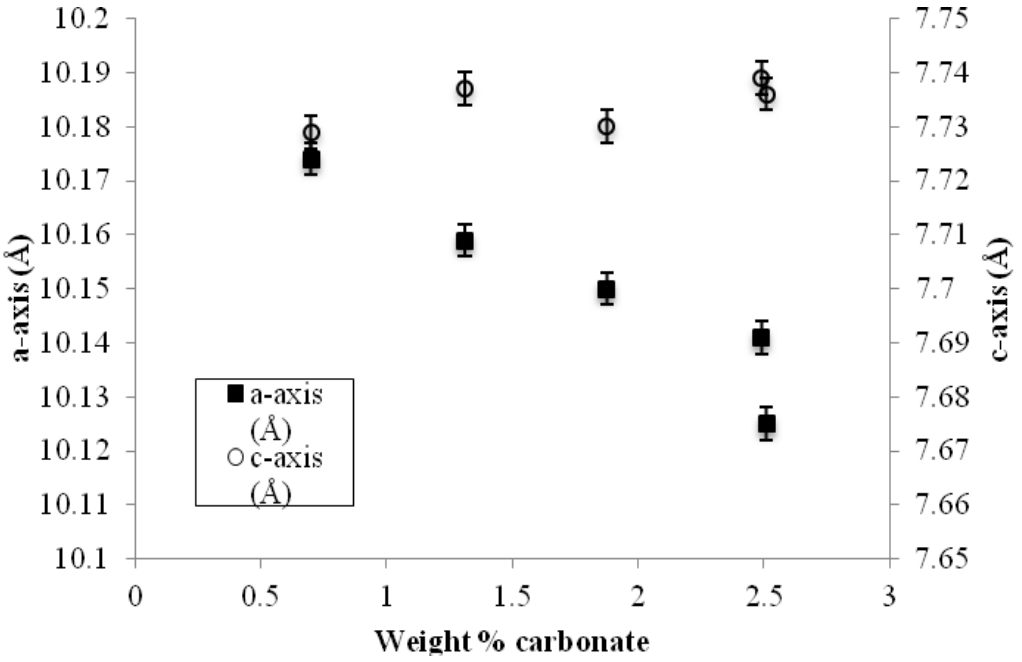

787

788 Fig. 1

789

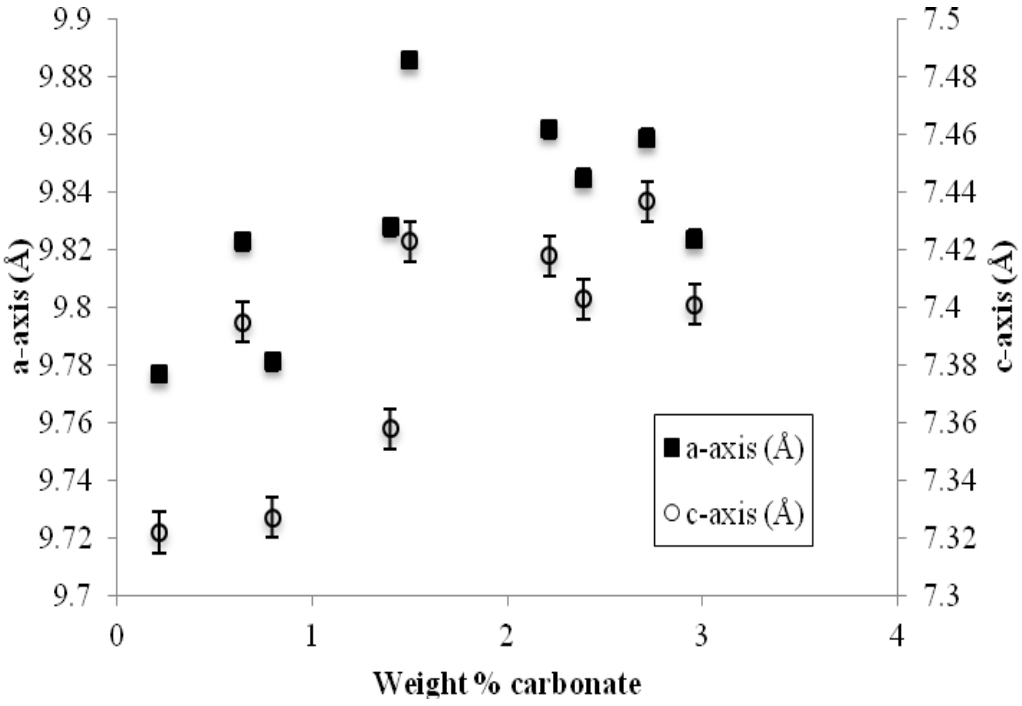

790

791

792 Fig. 2

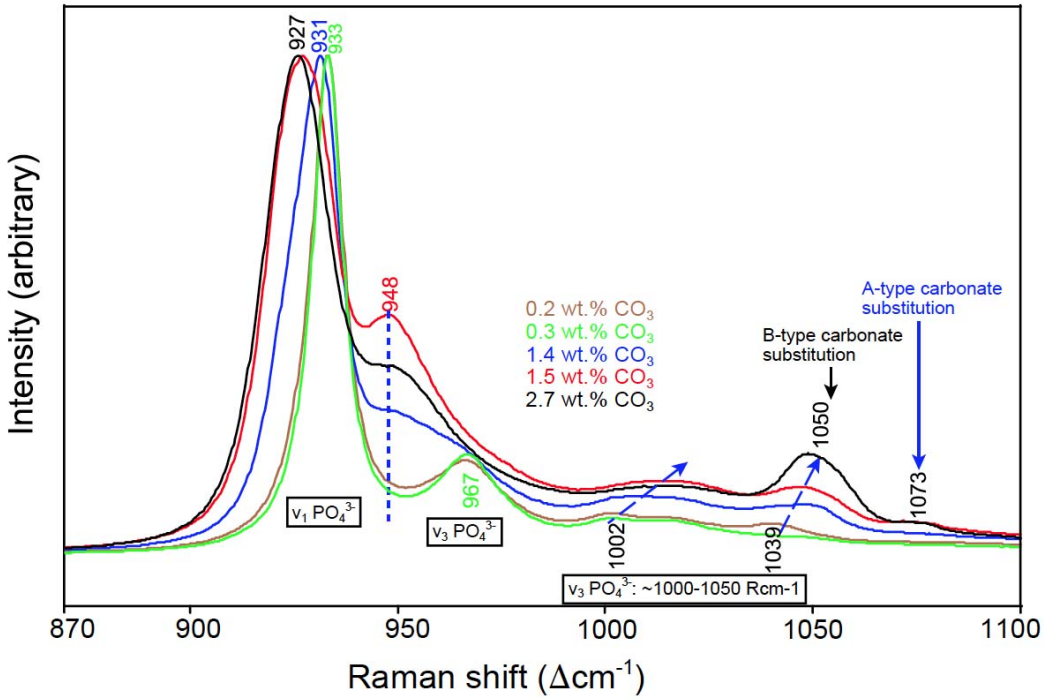

793

794 Fig. 3

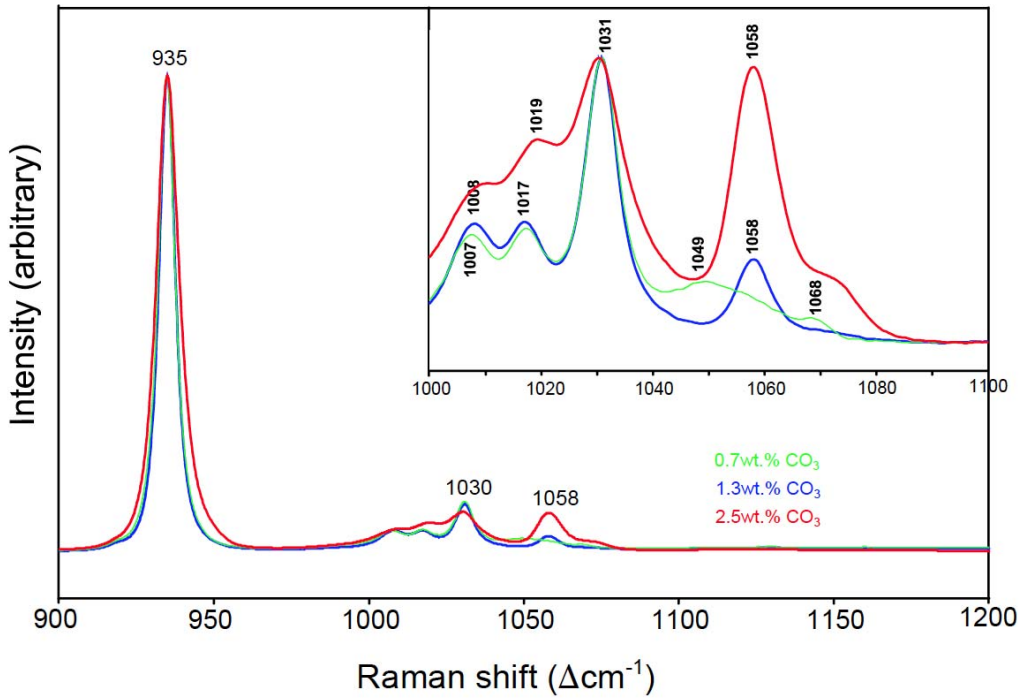

795

796 Fig. 4

797

798

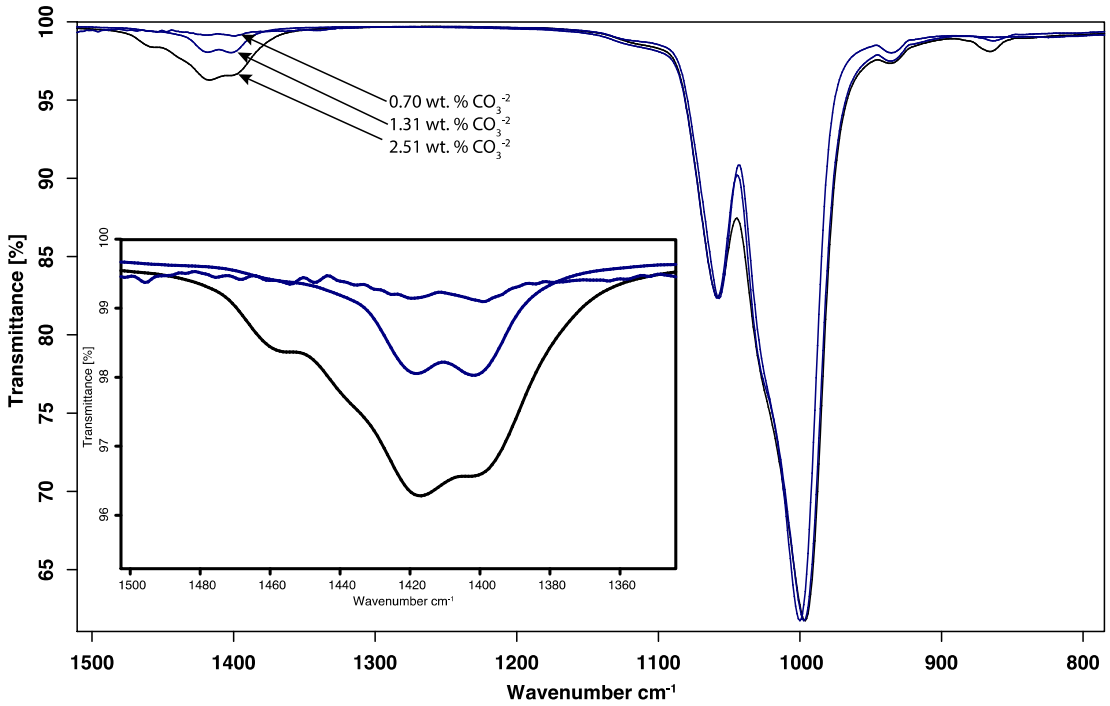

799

800 Fig. 5

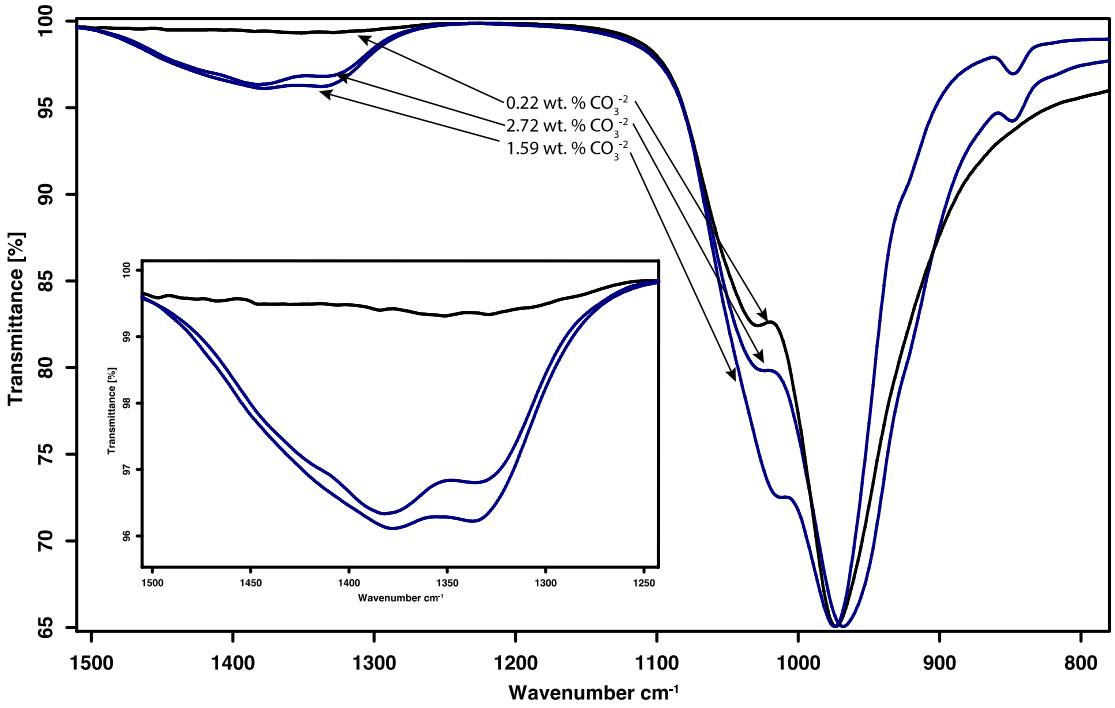

801

802 Fig. 6

803

804

805

806

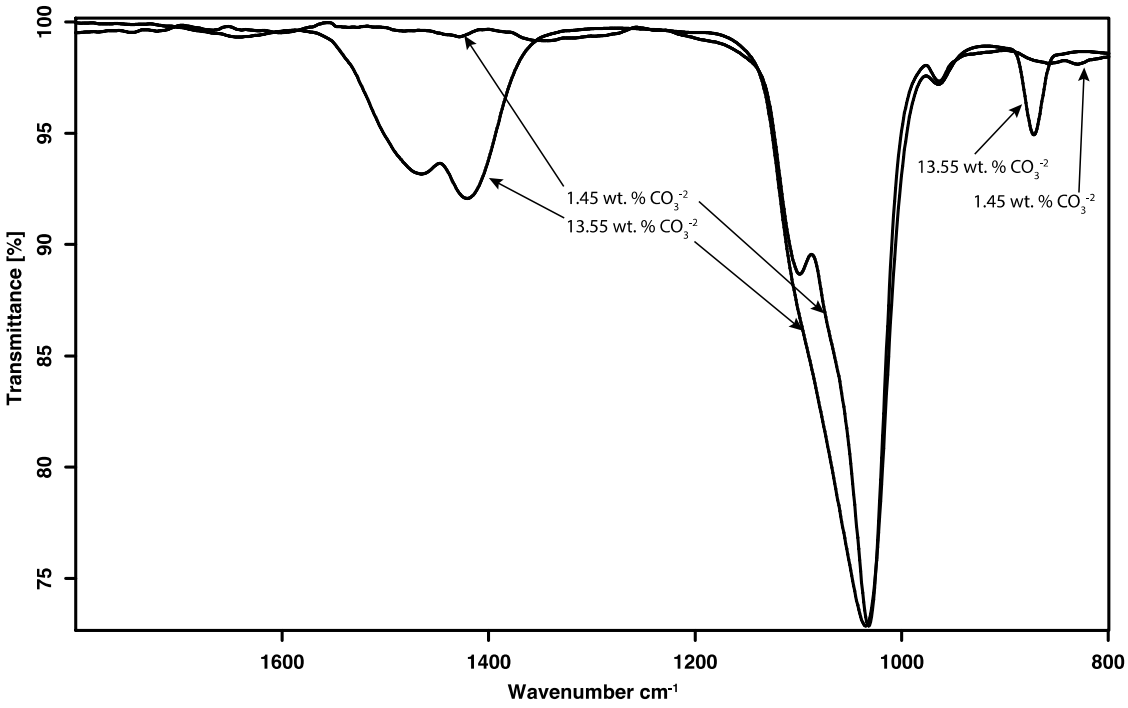

807

808
809 Fig. 7
810
811
812
813